magnetochemistry

MDPI

Communication

Magnetite–Corrole Hybrid Nanoparticles

Rute A. Pereira [1], Tito Trindade [1] and Joana F. B. Barata [1,2,*]

[1] Department of Chemistry and CICECO, University of Aveiro, 3800-193 Aveiro, Portugal; rute.pereira@ua.pt (R.A.P.); tito@ua.pt (T.T.)
[2] Department of Chemistry and QOPNA, University of Aveiro, 3800-193 Aveiro, Portugal
* Correspondence: jbarata@ua.pt; Tel.: +351-234-370-200

Received: 22 June 2018; Accepted: 17 August 2018; Published: 22 August 2018

Abstract: This study describes the first example of a hybrid material comprising corrole- and silica-coated magnetite nanoparticles. Firstly, cuboid and spheroid magnetite nanoparticles were prepared using a simple hydrothermal route, followed by a silica coating. The hybrid nanoparticles were obtained by promoting a covalent link between a gallium (III)(pyridine) complex of 5,10,15-tris(pentafluorophenyl)corrole (GaPFC) and the surface of magnetite–silica core/shell nanoparticles (Fe_3O_4@SiO_2), shaped both as cuboids and spheroids. The hybrids were characterized using Fourier transform infrared spectroscopy (FTIR), X-ray diffraction (XRD), ultraviolet-visible spectrophotometry (UV-Vis) and transmission electron microscopy (TEM). Preliminary studies on the capacity of singlet oxygen generation of the hybrid nanoparticles showed that these have lower efficiency values when compared to the pure corrole compound.

Keywords: magnetite nanoparticles; corroles; photodynamic therapy

1. Introduction

Corroles are aromatic tetrapyrrolic ring-contracted macrocycles that have attracted considerable attention due to their interesting and unique properties. Recent developments on chemical functionalization approaches of corroles have given new impetus to the application of these compounds in several areas [1–6]. For example, they are used in the therapeutic field as inactivation agents for bacteria, viruses, and fungi; contrast agents for biomedical imaging; photosensitizers for photodynamic therapy to fight cancer [7–16]; and also as catalysts [5] and sensors [4].

The preparation of corrole nanoconjugates—envisaging multifunctional nanometer-scale materials with key photophysical properties to be used in areas devoted to nanotechnology—has been unexplored, with few examples in the literature. For instance, corrole–TiO_2 hybrids have been used as contrast agents and dye-sensitized solar cells [17,18]; corrole–silica particles were studied as photosensitizers in photodynamic therapy [19]; and conjugates of Quantum Dots with gold(III) corroles were prepared for sensing applications [20].

In regard to different types of nanoparticles, iron oxide nanoparticles have attracted increasing interest due to their unique and novel physiochemical properties [21] in a wide range of fields, including catalysis [21], biological applications such as MRI (magnetic resonance imaging), and targeted drug delivery [22–24].

Magnetite (Fe_3O_4)—one of the most used magnetic materials—has been used as a solid support to immobilize porphyrin macrocycles using different synthetic approaches. For instance, TCPP(a porphyrin derivative)-PEG(poly(ethylene glycol))-functionalized magnetic nanoparticles were prepared using PEG as a ligand for the immobilization of porphyrin. These hybrids were tested as nanocatalysts in the degradation of Bisphenol A [24]. Other studies have reported the use of a silica shell as the key to promote the chemical grafting between porphyrin and magnetite nanoparticles, e.g.,

by nucleophilic substitution of crucial porphyrinic groups with the amino surface of magnetite–silica core/shell nanoparticles [25,26] or via carbodiimide activation [27,28]. These hybrids were evaluated as antibacterial agents [26,29], as photocatalysts [30], as magnetic heavy metal ions adsorbents [27], and as adsorbents for polycyclic aromatic hydrocarbons from water samples [31].

The preparation of porphyrin–magnetite hybrids prompted us to perform the chemical synthesis of hybrids composed of magnetite nanoparticles and a corrolic macrocycle. This combination of iron oxide nanoparticles and corrole has not yet been explored. Taking into account our previous report on the preparation of corrole-functionalized SiO_2 nanoparticles [19], we decided to carry out the chemical grafting of functionalized gallium(III)(pyridine) complex of 5,10,15-tris(pentafluorophenyl)corrole (GaPFC) with core/shell magnetite–silica nanoparticles (Fe_3O_4@SiO_2) in a two-step approach. A preliminary evaluation of its potential as photosensitizer for photodynamic therapies was briefly assessed through the determination of its capacity to generate singlet oxygen.

2. Results and Discussion

Figure 1 illustrates the synthetic route employed to obtain the hybrid nanoparticles. Although there has been no attempt to detail the structural features in this scheme (Figure 1), it should be noted that the pentafluorophenyl rings are not coplanar in relation to the corrole macrocycle [3]. In order to minimize side reactions, namely inner core reactions, the gallium(III)(pyridine) complex of 5,10,15-tris(pentafluorophenyl)corrole (GaPFC) [32] was selected as a stable metal-coordinated corrole derivative. We favored this aspect despite the limitations GaPFC might have as a photosensitizer for singlet oxygen generation when compared, for example, to free corrole.

Fe_3O_4 nanoparticles were synthesized according to standard procedures that resulted in either cuboid or spheroid magnetic nanoparticles [33,34]. The cuboid nanoparticles were prepared as described by Girginova et al. [33] by hydrolysis of $FeSO_4 \cdot 7H_2O$ in the presence of potassium nitrate and potassium hydroxide. Spheroid nanoparticles were synthesized by oxidative hydrolysis of $FeSO_4 \cdot 7H_2O$ under alkaline conditions as described by Oliveira-Silva et al. [34]. The obtained magnetite nanoparticles were then coated with amorphous silica shells.

The core/shell nanoparticles were functionalized with GaPFC in a two-step procedure: In the first step, a nucleophilic substitution reaction was promoted between the para-fluorine atoms of pentafluorophenyl rings of GaPFC with (3-aminopropyl)triethoxysilane (APTES) [19]. In the second step, silica-coated Fe_3O_4 nanoparticles were added to the previous mixture in order to promote the chemical grafting of GaPFC previously functionalized with APTES.

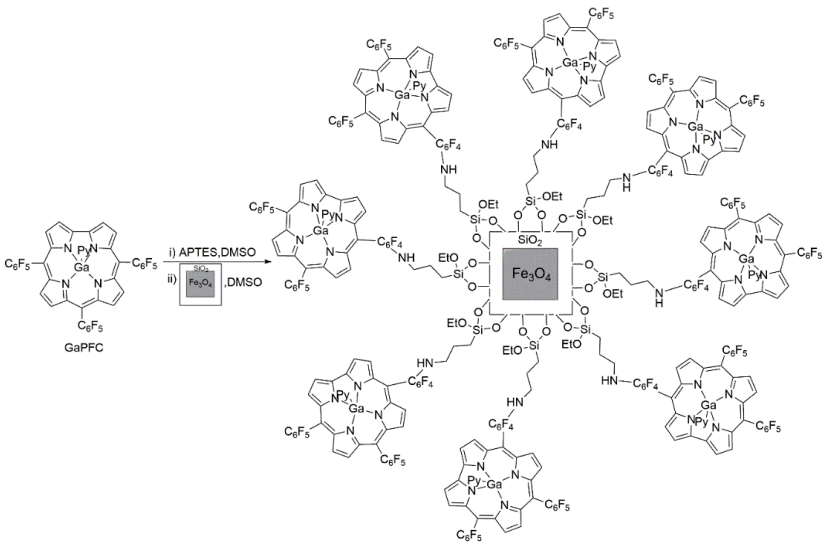

Figure 1. Synthetic routes to magnetite–corrole hybrid nanoparticles.

The resulting solids were then filtered and washed with an appropriated solvent in order to remove the unbound corrole. This process was monitored by recording the UV-Vis spectra of the supernatant until no absorbance was observed in the range of 300–800 nm.

Infrared Spectroscopy was used as a characterization technique to identify typical chemical bonds within the structure of the prepared magnetite and hybrid nanoparticles. Table 1 indicates the main vibrational bands in the FTIR/ATR spectra (FTIR Bruker Tensor 27, Bruker, Billerica, MA, USA) of cuboid and spheroid Fe_3O_4 nanoparticles and for the respective corrole functionalized derivatives. The FTIR spectra for magnetite nanoparticles showed a vibrational band near 536 cm^{-1} ascribed to the Fe–O stretching mode. For core/shell nanoparticles, the vibrational bands between 551 and 558 cm^{-1} were also ascribed to the Fe–O stretching mode. In addition, typical vibrational bands for amorphous silica were observed in the 773–785 cm^{-1} and 1002–1028 cm^{-1} regions due to symmetric Si–O–Si and asymmetric Si–O–Si stretching vibration mode, respectively [35]. Vibrational bands of less intensity were also observed at 1400–1600 cm^{-1}, which could be assigned to the corrole macrocycle and the characteristic stretching modes of pyrrole ($n_{C–H}$, $n_{C–C}$, and $n_{C–N}$) observed in the 700–1500 cm^{-1} range [19]. In summary, the FTIR/ATR vibrational data indicated the presence of all the components employed to form the hybrid magnetic nanoparticles.

Table 1. FTIR/ATR vibrational bands and respective assignments for all the prepared nanoparticles and hybrids.

	536 cm^{-1}	551–558 cm^{-1}	773–785 cm^{-1}	1002–1028 cm^{-1}	1400–1600 cm^{-1}	700–1500 cm^{-1}
Cuboid and spheroid Fe_3O_4	ν(Fe–O)	-	-	-	-	-
Cuboid and spheroid Fe_3O_4@SiO_2	-	ν(Fe–O)	ν(Si–O–Si)	ν(Si–O–Si)	-	-
Cuboid and spheroid Magnetite–corrole Hybrid nanoparticles	-	ν(Fe–O)	ν(Si–O–Si)	ν(Si–O–Si)	n(C–H), n(C–C), n(C–N)	n(C–H), n(C–C), n(C–N)

In order to confirm the presence of the corrole macrocycle linked onto the surface of Fe_3O_4@SiO_2 nanoparticles, the UV-Vis spectra of the hybrid nanoparticles in ethanol were collected. Figure 2 shows that both cuboid (Figure 2a) and spheroid (Figure 2b) magnetic functionalized samples exhibited the characteristic Soret band of GaPFC but redshifted from 419 nm to 424 nm in relation to the pure complex. The background signal of the absorbance curves was due to light scattering and is typical of aggregated nanoparticles. In fact, this might have been an indication that the GaPFC molecules grafted at the SiO_2 surfaces of the core/shell nanoparticles were interacting due to their proximity as a consequence of particle aggregation. The broadening of the Q band at 602 nm (for cuboid particles) and 607 nm (for spheroid particles) in the UV-Vis spectra of the hybrids was also consistent with aggregation effects occurring in the colloidal functionalized particles in ethanol.

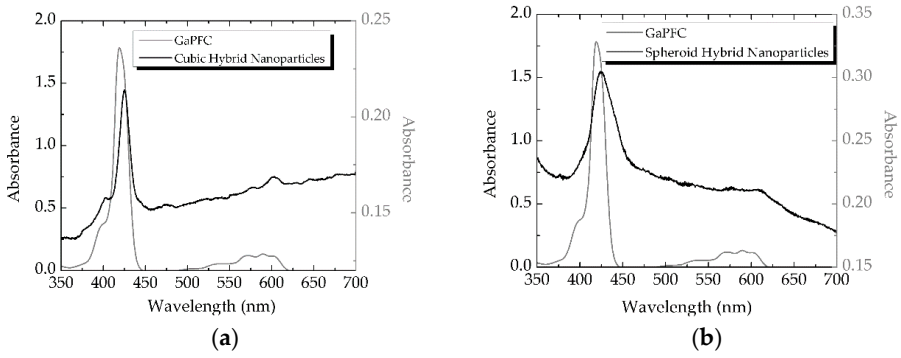

Figure 2. UV-VIS spectra in ethanol of (**a**) cuboid hybrid nanoparticles and (**b**) spheroid hybrids hybrid nanoparticles and respective corrole precursor.

Fe_3O_4, Fe_3O_4@SiO_2, and hybrid nanoparticles were also analyzed by powder X-ray diffraction (XRD, Empyrean powder diffractometer, PANalytical, Almelo, The Netherlands) in order to identify the desired inorganic phase (Fe_3O_4). The obtained patterns are shown in Figure 3, which confirmed that magnetite (Fe_3O_4) was the main crystal phase present in both cuboid and spheroid nanoparticles (Figure 3a,d). Of course, small amounts of maghemite could not be discarded, since both magnetite and maghemite have a spinel structure and exhibit very similar powder XRD patterns. However, the obtained powder was black, which confirmed the presence of magnetite and not maghemite nanoparticles, which are typically brown. The same pattern could be observed in core/shell nanoparticles (Figure 3b,e) and in the hybrids (Figure 3c,f).

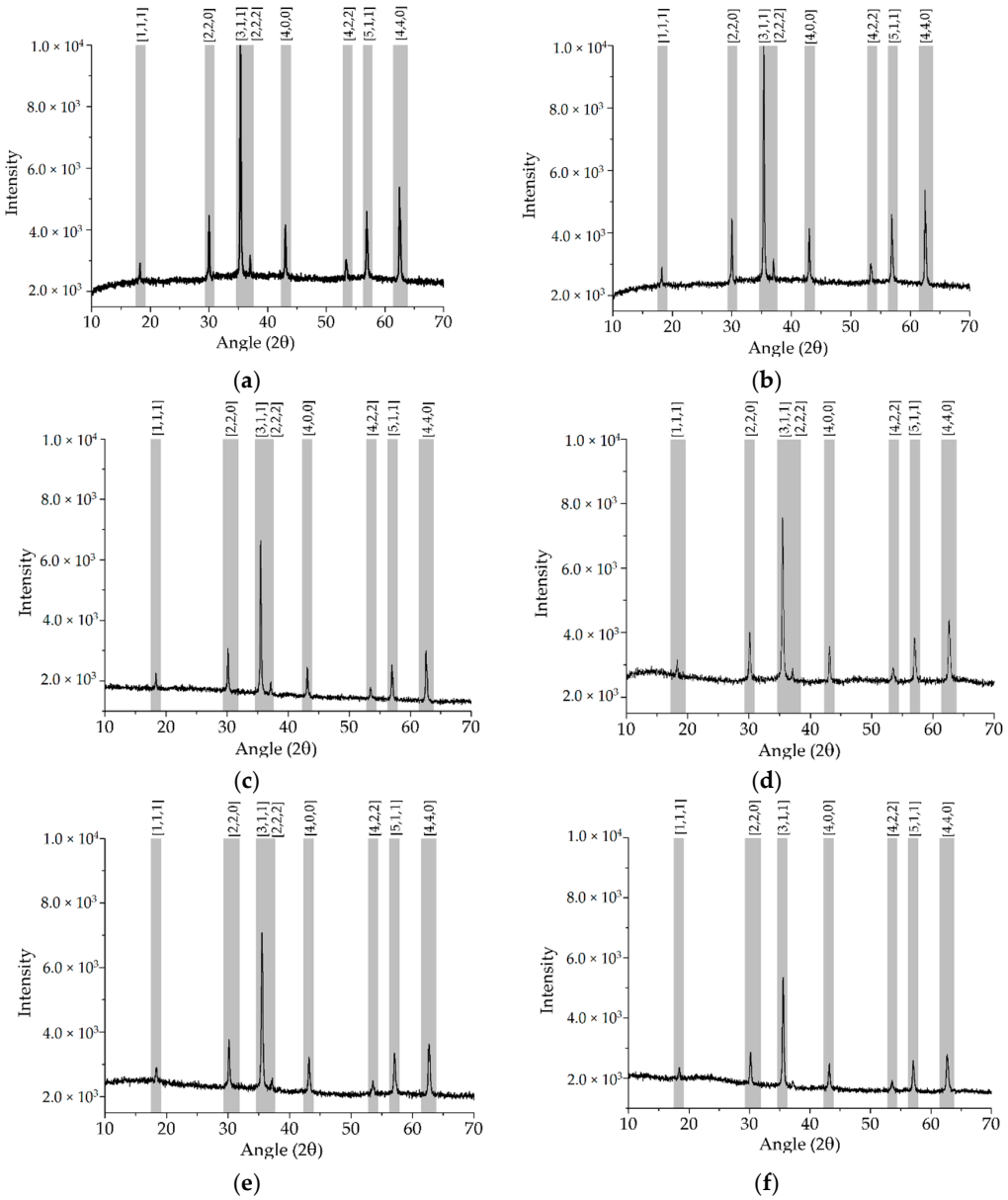

Figure 3. X-ray diffractograms of (**a**) cuboid Fe_3O_4 nanoparticles, (**b**) cuboid Fe_3O_4@SiO_2 nanoparticles, (**c**) cuboid hybrid nanoparticles, (**d**) spheroid Fe_3O_4 nanoparticles, (**e**) spheroid Fe_3O_4@SiO_2 nanoparticles, and (**f**) spheroid hybrid nanoparticles.

The morphological characteristics of the Fe_3O_4, Fe_3O_4@SiO_2, and hybrid nanoparticles were analyzed by transmission electron microscopy (TEM, Hitachi H9000, Hitachi, Chiyoda, Tokyo, Japan), as shown in Figure 4. Both Fe_3O_4 nanoparticles samples were relatively polydisperse, with the cuboid Fe_3O_4 nanoparticles (Figure 4a) showing an average size of about 89 nm, whereas the spheroid Fe_3O_4 nanoparticles (Figure 4d) presented an average size of 50 nm. The thickness of the silica shells in both cases varied between 14 and 18 nm, respectively (Figure 4b,e), after chemical grafting with GaPFC previously functionalized with APTES (Figure 4c,f). In these images, the nanoparticles seem to be more aggregated, which is in line with the optical spectra discussed above and the clustering effect, a consequence of the GaPFC attached at the silica particle surfaces, as previously reported [19].

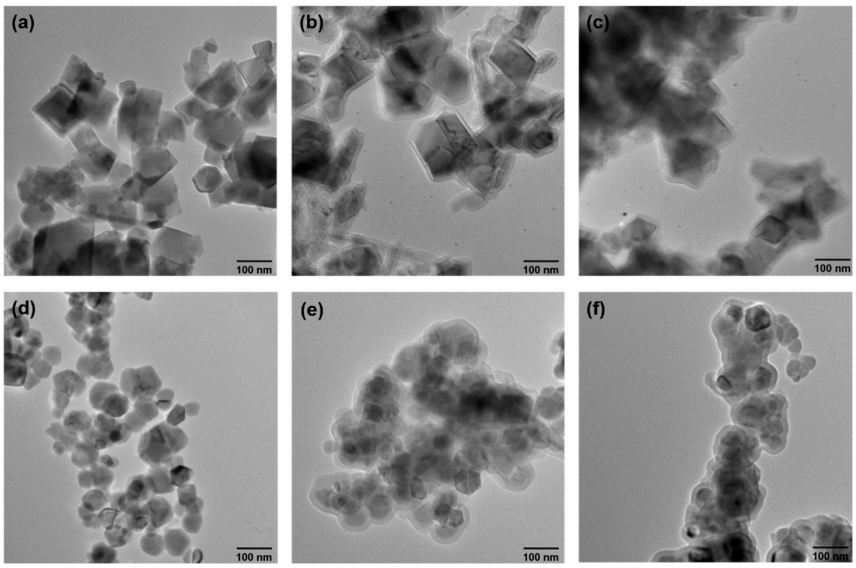

Figure 4. TEM images of the nanoparticle samples employed in this research: (**a**) cuboid Fe_3O_4, (**b**) cuboid Fe_3O_4@SiO_2, (**c**) Cuboid Fe_3O_4@SiO_2 functionalized with corrole molecules, (**d**) Spheroid Fe_3O_4, (**e**) Spheroid Fe_3O_4@SiO_2, (**f**) Spheroid Fe_3O_4@SiO_2 functionalized with corrole molecules.

As a complementary work, the potential of the developed hybrid nanoparticles as photosensitizers was preliminarily evaluated by estimating the capacity to generate singlet oxygen ($^1O_2$) using 1,3-diphenylisobenzofuran (DPiBF) as a $^1O_2$ indicator [19]. Briefly, the UV-Vis absorbance decay at 415 nm was measured as the oxidation of DPiBF in the presence of $^1O_2$, which occurs via Diels–Alder cycloaddition affording colorless *o*-dibenzoylbenzene. Here, there were no attempts to detail the photophysics involved in these systems but instead provide a preliminary assessment of the functionalized corrole magnetic nanoparticles to generate $^1O_2$. Table 2 shows the DPiBF absorption decay at 415 nm after DMF suspensions of DPiBF and after the hybrid nanoparticles (or the GaPFC) had been irradiated with red light at a fluence rate of 25 $W \cdot m^{-2}$. The GaPFC produced about 80% of $^1O_2$, proving to be a strong photosensitizer even in small concentrations, in the irradiated solution. It is clear from these results that the hybrid nanoparticles—both cuboid and spheroid—might be able to generate $^1O_2$, although with a lower efficiency compared to free GaPFC complex. The higher efficiency of the spheroid hybrid compared to the cuboid analogue might be related to the higher superficial area of spheroid nanoparticles.

Table 2. Singlet oxygen generation assays.

Photosensitizer	DPiBF Decay (%)
GaPFC (0.008mg/mL)	80
Cuboid hybrid nanoparticles (0.231 mg/mL)	15
Spheroid hybrid (0.242 mg/mL)	25

3. Materials and Methods

3.1. Chemicals

(3-aminopropyl)triethoxysilane (APTES) ($H_2N(CH_2)_3Si(OC_2H_5)_3$) (Sigma-Aldrich, St. Louis, MO, USA, 98.8%); Ammonia (NH_4OH) (Sigma-Aldrich, 33%); 2,3-dichloro-5,6-dicyano-p-benzoquinone (DDQ) ($C_8Cl_2N_2O_2$) (Sigma-Aldrich, 98%); dichloromethane (CH_2Cl_2) (Sigma-Aldrich, 99.9%); dimethylformamide (DMF) ($(CH_3)_2NCHO$, 99.99%, Fisher Scientific, Hampton, NH, USA), ethanol (C_2H_6O) (Fisher Chemical, Hampton, NH, USA, 99.99%); iron (II) sulfate heptahydrate ($FeSO_4{\cdot}7H_2O$) (Sigma-Aldrich, >99%); potassium hidroxide (KOH) (LABCHEM, Zelienople, PA, USA, lentils, pure); potassium nitrate (KNO_3) (LABCHEM, Zelienople, PA, USA, lentils, pure); tetraethylorthosilicate (TEOS) ($Si(OC_2H_5)_4$) (Sigma Aldrich, 99%); tetrahydrofuran (THF) (C_4H_8O) (Sigma-Aldrich, 99.0%); toluene (C_7H_8) (Sigma-Aldrich, 99.8%); trifluoroacetic acid (TFA) ($C_2HF_3O_2$) (Sigma-Aldrich, 99%), 1,3-diphenylisobenzofuran (DPiBF) (95%, Sigma-Aldrich) pentafluorobenzaldehyde (CF5CHO, 95%, Sigma-Aldrich) and gallium(III) chloride ($GaCl_3$, 99%, Sigma-Aldrich) were used as received.

Pyrrole (C_4H_4NH, 95%, Sigma-Aldrich) was distilled before use. Toluene (C_7H_8) (Sigma-Aldrich, 99.8%); dimethyl sulfoxide (DMSO) (C_2H_6OS) (Sigma-Aldrich, 99.99%); and pyridine (Fluka) were dried using standard procedures. Ultrapure deionized water (resistivity > 8 Ω cm) was used for preparing the aqueous solutions.

3.2. Syntheses

The gallium(III)(pyridine) complex of 5,10,15-tris(pentafluorophenyl)corrole (GaPFC) was prepared by complexation of the corresponding free base 5,10,15-tris-(pentafluorophenyl)corrole with $GaCl_3$ in refluxing pyridine according to the literature [33]. The free base was synthesized by condensation of pyrrole with pentafluorobenzaldehyde using the Gryko's method [36].

Cuboid nanoparticles with an average size of 89 nm were prepared as described by Girginova et al., via hydrolysis of $FeSO_4{\cdot}7H_2O$ using potassium nitrate and potassium hydroxide [33]. Typically, in a 250 mL round bottom flask containing 70 mL of deionized and deaerated water, 10 g of $FeSO_4{\cdot}7H_2O$ were added, followed by a dropwise addition of an aqueous solution (30 mL) of KNO_3 (0.81 g) and KOH (5.625 g). After one hour at 87 °C and under mechanical stirring, the obtained suspension was left overnight at room temperature without stirring. The resulting magnetite nanoparticles were then decanted and washed with deionized water and then with ethanol.

Spheroid nanoparticles with an average size of 50 nm were synthesized by oxidative hydrolysis of $FeSO_4{\cdot}7H_2O$ under alkaline conditions, as described by Oliveira-Silva et al [34]. In a typical synthesis, 1.90 g of KOH and 1.52 g of KNO_3 were added to a 250 mL round-bottom flask containing 25 mL of deaerated water. The obtained mixture was heated at 60 °C, under an atmosphere of N_2, and mechanically stirred (500 rpm). After complete dissolution of the salt, 25 mL of an aqueous solution containing 4.75 g of $FeSO_4{\cdot}7H_2O$ was added dropwise under an increased stirring (700 rpm), and the resulting reacting mixture was left over 30 min. Afterwards, this mixture was maintained at 90 °C and left under an N_2 atmosphere without stirring over 4 h.

3.3. Surface Functionalization

The surface of cuboid and spheroid nanoparticles were then coated with amorphous SiO_2 [33]. Hence, 80 mL of ethanol containing 100 mg of magnetite nanoparticles were sonicated for 20 min using

an ice bath. Afterwards, 6 mL of ammonia and 200 μL of TEOS were added, and the mixture was sonicated over 2 h. The resulting SiO_2-coated magnetite nanoparticles were then decanted and washed with deionized water and then with ethanol. These particles were functionalized with corrole as follows:

GaPFC (20 mg, 2.32×10^{-5} mol) was added to APTES (50 μL, 2.32×10^{-5} mol) and $CsCO_3$ (7 mg, 2.32×10^{-5} mol) in dry DMSO (2 mL), and the resulting mixture was magnetically stirred during 3 days at 40 °C under N_2 atmosphere. Afterwards, 100 mg of SiO_2-coated magnetite nanoparticles were added with an additional 2 mL of DMSO. The reaction mixture was then stirred at room temperature for 2 days. In order to remove the excess of nonreacted corrole, the hybrid nanoparticles were thoroughly washed with ethanol and magnetically separated, a process which was monitored by recording the UV-Vis spectra of the supernatant until no absorbance in the range of 300–800 nm was detected.

3.4. Instrumentation

The FTIR/ATR spectra were recorded using a Mattson 7000 spectrometer at 4 cm^{-1} resolution.

Powder X-ray diffraction was performed in the range of 10°–70° 2θ on a PANalytical Empyrean diffractometer using $k_{\alpha 1}$ Copper radiation with λ = 1.54060 Å.

The TEM samples were prepared by depositing diluted suspensions of the particles on a copper grid, after sonication dispersion, and the solvent was left to evaporate. The samples were analyzed using a Hitachi H8100 II microscope (Hitachi H9000, Hitachi, Chiyoda, Tokyo,) at 200 kV voltage.

The UV-Vis absorption measurements were carried out by using a UV-Vis GBC CINTRAL 303 spectrophotometer (GBC Scientific Equipment, Braeside, Victoria, Australia).

The fluorescence emission measurements were performed using a Jasco FP-830 spectrofluorometer (JASCO Corporation, Easton, MD, USA).

The singlet oxygen production was assessed using a plate of red LEDs (λ = 625 ± 15 nm) at 20 mW/cm^2, and the absorption of DPiBF was measured in a Shimazu UV-2501PC spectrophotometer (Shimadzu Corporation, Kyoto, Japan). A stock suspension of hybrid nanoparticles at 0.01 mM in DMF, stock solutions of the gallium(III)(pyridine) complex of 5,10,15-tris(pentafluorophenyl)corrole (GaPFC) at 10.6 μM and at 568 mM (corresponding to the expected concentration of GaPFC present in the hybrid) and of DPiBF at 10 mM in DMF were prepared. Reaction mixtures of 50 μM of DPiBF and 0.008 mg/mL of GaPFC and 0.231 mg/mL in DMF were irradiated in a quartz cell (2.5 mL) with a red light (λ = 625 ± 15 nm) at a fluence rate of 25 W/m^2. During the irradiation period, the solutions were stirred at room temperature, and the generation of singlet oxygen was followed by an indirect method that involves the reaction with DPiBF. The breakdown of DPiBF was monitored by measuring the decrease in the absorbance at 415 nm, at irradiation intervals of 2 min for 14 min. The percentage of the DPiBF absorption decay, which is proportional to the production of singlet oxygen, was monitored by measuring the difference between the initial absorbance at 415 nm and the absorbance after the required time of irradiation.

4. Conclusions

Corrole–magnetite hybrid nanoparticles were successfully prepared using a methodology that led to a covalent bond between a gallium(III)(pyridine) complex of 5,10,15-tris(pentafluorophenyl)corrole (GaPFC) and the surface of silica-coated magnetite. The hybrid nanoparticles were obtained in both cuboid and spheroid shapes. Keeping in mind the same areas of application as their porphyrinic counterparts, especially their use as photosensitizers, the preliminary assay on the evaluation of the generation of singlet oxygen showed potential to be used as photosensitizers. However, some issues must be further addressed, such as the aggregation of the hybrids. The biological activity should also be studied against cancer cell lines if or against bacterial strains for antimicrobial photodynamic therapy.

Author Contributions: This work was conceptualized by J.F.B.B. and T.T. The methodology was developed by R.A.P. under the supervision of J.F.B.B. and T.T. The obtained results were validated by J.F.B.B. and T.T. The writing original draft preparation was carried out by R.A.P. and J.F.B.B. The writing was reviewed and edited by T.T.

Funding: This research was funded by the project CICECO—Aveiro Institute of Materials, POCI-01-0145-FEDER-007679 (Ref. UID/CTM/50011/2013), financed by national funds through the FCT/MEC and when appropriate, co-funded by the European Regional Development Fund (FEDER) under the PT2020 Partnership Agreement. J.F.B.B. thanks FCT for the grant SFRH/BPD/63237/2009). The authors wish to thank Fundação para a Ciência e a Tecnologia (FCT), FSE, and POPH for funding the Organic Chemistry Research Unit (Pest-C/QUI/UI0062/2011).

Acknowledgments: We thank RNME (National Electronic Microscopy Network) for the TEM images. The authors wish to thank Ana Maria Farinha for the help in designing the cover image.

Conflicts of Interest: The authors declare no conflict of interest.

References

1. Barata, J.F.B.; Neves, M.G.P.M.S.; Faustino, M.A.F.; Cavaleiro, J.A.S. Strategies for corrole functionalization. *Chem. Rev.* **2017**, *117*, 3192–3253. [CrossRef] [PubMed]
2. Santos, C.I.M.; Oliveira, E.; Barata, J.F.B.; Faustino, M.A.F.; Cavaleiro, J.A.S.; Neves, M.G.P.M.S.; Lodeiro, C. Corroles as Anion Chemosensors: Exploiting Their Fluorescence Behaviour from Solution to Solid-Supported Devices. *J. Mater. Chem.* **2012**, *22*, 13811–13819. [CrossRef]
3. Santos, C.I.M.; Oliveira, E.; Barata, J.F.B.; Faustino, M.A.F.; Cavaleiro, J.A.S.; Neves, M.G.P.M.S.; Lodeiro, C. New gallium(III) Corrole Complexes as Colorimetric Probes for Toxic Cyanide Anion. *Inorg. Chim. Acta* **2014**, *417*, 148–154. [CrossRef]
4. Sheng, X.; Zhao, H.; Du, L. Selectivity of Cobalt Corrole for CO vs. O_2 and N_2 in Indoor Pollution. *Sci. Rep.* **2017**, *7*, 14536. [CrossRef] [PubMed]
5. Zhang, W.; Lai, W.; Cao, R. Chemical Energy-Related Small Molecule Activation Reactions: Oxygen Reduction and Hydrogen and Oxygen Evolution Reactions Catalyzed by Porphyrin- and Corrole-Based Systems. *Chem. Rev.* **2017**, *117*, 3717–3797. [CrossRef] [PubMed]
6. Paolesse, R.; Nardis, S.; Monti, D.; Stefanelli, M.; Di Natale, C. Porphyrinoids for Chemical Sensor Applications. *Chem. Rev.* **2016**, *117*, 2517–2583. [CrossRef] [PubMed]
7. Teo, R.D.; Hwang, J.Y.; Termini, J.; Gross, Z.; Gray, H.B. Fighting Cancer with Corroles. *Chem. Rev.* **2017**, *117*, 2711–2729. [CrossRef] [PubMed]
8. Barata, J.F.B.; Pinto, R.J.B.; Vaz Serra, V.I.R.C.; Silvestre, A.J.D.; Trindade, T.; Neves, M.G.P.M.S.; Cavaleiro, J.A.S.; Daina, S.; Sadocco, P.; Freire, C.S.R. Fluorescent Bioactive Corrole Grafted-Chitosan Films. *Biomacromolecules* **2016**, *17*, 1395–1403. [CrossRef] [PubMed]
9. Pohl, J.; Saltsman, I.; Mahammed, A.; Gross, Z.; Roder, B. Inhibition of Green Algae Growth by Corrole-Based Photosensitizers. *J. Appl. Microbiol.* **2015**, *118*, 305–312. [CrossRef] [PubMed]
10. Sims, J.D.; Hwang, J.Y.; Wagner, S.; Alonso-Valenteen, F.; Hanson, C.; Taguiam, J.M.; Polo, R.; Harutyunyan, I.; Karapetyan, G.; Sorasaenee, K.; et al. A Corrole Nanobiologic Elicits Tissue-Activated MRI Contrast Enhancement and Tumor-Targeted Toxicity. *J. Control. Release* **2015**, *217*, 92–101. [CrossRef] [PubMed]
11. Samaroo, D.; Perez, E.; Aggarwal, A.; Wills, A.; O'Connor, N. Strategies for Delivering Porphyrinoid-Based Photosensitizers in Therapeutic Applications. *Ther. Deliv.* **2014**, *5*, 859–872. [CrossRef] [PubMed]
12. Preuß, A.; Saltsman, I.; Mahammed, A.; Pfitzner, M.; Goldberg, I.; Gross, Z.; Roder, B. Photodynamic Inactivation of Mold Fungi Spores by Newly Developed Charged Corroles. *J. Photochem. Photobiol. B* **2014**, *133*, 39–46. [CrossRef] [PubMed]
13. Pribisko, M.; Palmer, J.; Grubbs, R.H.; Gray, H.B.; Termini, J.; Lim, P. Cellular Uptake and Anticancer Activity of Carboxylated Gallium Corroles. *Proc. Natl. Acad. Sci. USA* **2016**, *113*, E2258–E2266. [CrossRef] [PubMed]
14. Aviv-Harel, I.; Gross, Z. Aura of Corroles. *Chem. Eur. J.* **2009**, *15*, 8382–8394. [CrossRef] [PubMed]
15. Haber, A.; Angel, I.; Mahammed, A.; Gross, Z. Combating Diabetes Complications by 1-Fe, a Corrole-Based Catalytic Anti-oxidant. *J. Diabetes Complicat.* **2013**, *27*, 316–321. [CrossRef] [PubMed]
16. Barata, J.F.B.; Zamarron, A.; Neves, M.G.P.M.S.; Faustino, M.A.F.; Tomé, A.C.; Cavaleiro, J.A.S.; Röder, B.; Juarranz, A.; Sanz-Rodriiguez, F. Photodynamic effects induced by meso-tris(pentafluorophenyl)corrole and its cyclodextrin conjugates on cytoskeletal components of HeLa cells. *Eur. J. Med. Chem.* **2015**, *92*, 135–144. [CrossRef] [PubMed]

17. Blumenfeld, C.; Sadtler, B.; Fernandez, G.; Dara, L.; Nguyen, C.; Alonso-Valenteen, F.; Medina-Kauwe, L.; Moats, R.; Lewis, N.; Grubbs, R.; et al. Cellular uptake and cytotoxicity of a near-IR fluorescente corrole-TiO_2 nanoconjugate. *J. Inorg. Biochem.* **2014**, *140*, 39–44. [CrossRef] [PubMed]
18. Sudhakar, K.; Giribabu, L.; Salvatori, P.; de Angelis, F. Triphenylamine-functionalized corrole sensitizers for solar-cell applications. *Phys. Status Solidi A* **2015**, *212*, 194–202. [CrossRef]
19. Barata, J.F.B.; Daniel-da-Silva, A.L.; Neves, M.G.P.M.S.; Cavaleiro, J.A.S.; Trindade, T. Corrole-silica hybrid particles: Synthesis and effects on singlet oxygen generation. *RSC Adv.* **2013**, *3*, 274–280. [CrossRef]
20. Lemon, C.M.; Nocera, D.G. Comparison of self-assembled and micelle encapsulated QD chemosensor constructs for biological sensing. *Faraday Discuss.* **2015**, *185*, 249–266. [CrossRef] [PubMed]
21. Lu, A.H.; Salabas, E.L.; Schüth, F. Magnetic nanoparticles: Synthesis, protection, functionalization, and application. *Angew. Chem. Int. Ed.* **2007**, *46*, 1222–1244. [CrossRef] [PubMed]
22. Vaccari, C.B.; Cerize, N.N.P.; Morais, P.C.; Ré, M.I.; Tedesco, A.C. Biocompatible Magnetic Microscopheres for Use in PDT and Hyperthermia. *J. Nanosci. Nanotechnol.* **2012**, *12*, 5111–5116. [CrossRef] [PubMed]
23. Arruebo, M.; Fernández-Pacheco, R.; Ibarra, M.R.; Santamaría, J. Magnetic nanoparticles for drug delivery. *Nanotoday* **2007**, *2*, 22–32. [CrossRef]
24. Neamtu, M.; Nadejde, C.; Hodoroaba, V.; Schneider, R.; Panne, U. Singlet oxygen generation potential of porphyrin-sensitized magnetite nanoparticles: Synthesis, characterization and photocatalytic application. *Appl. Catal. B* **2018**, *232*, 553–561. [CrossRef]
25. Mak, C.; Pericas, M.; Fagadar-Cosma, E. Functionalization of A_3B-type porphyrin with Fe_3O_4 MNPs. Supramolecular assemblies, gas sensor and catalytic applications. *Catal. Today* **2018**, *306*, 268–275. [CrossRef]
26. Carvalho, C.M.B.; Alves, E.; Costa, L.; Tomé, J.P.C.; Faustino, M.A.F.; Neves, M.G.P.M.S.; Tomé, A.C.; Cavaleiro, J.A.S.; Almeida, A.; Cunha, Â.; Lin, Z.; Rocha, J. Functional Cationic Nanomagnet–Porphyrin Hybrids for the Photoinactivation of Microorganisms. *ACS Nano* **2010**, *4*, 7133–7140. [CrossRef] [PubMed]
27. Bakhshayesh, S.; Dehghani, H. Synthesis of magnetite-porphyrin nanocomposite and its application as novel magnetic adsorbent for removing heavy cations. *Mat. Res. Bull.* **2013**, *48*, 2614–2624. [CrossRef]
28. Scanone, A.C.; Gsponer, N.S.; Alvarez, M.G.; Durantini, E.N. Photodynamic properties and photoinactivation of microorganisms mediated by 5,10,15,20-tetrakis(4-carboxyphenyl)porphyrin covalently linked to silica-coated magnetite nanoparticles. *J. Photochem. Photobiol. A* **2017**, *346*, 452–461. [CrossRef]
29. Alves, E.; Rodrigues, J.; Faustino, M.; Neves, M.; Cavaleiro, J.; Lin, Z.; Cunha, Â.; Nadais, M.; Tomé, J.; Almeida, A. A new insight on nanomagnet-porphyrin hybrids for photodynamic inactivation of microorganisms. *Dyes Pigments* **2014**, *110*, 80–88. [CrossRef]
30. Rabbani, M.; Rafiee, F.; Ghafuri, H.; Rahimi, R. Synthesis of Fe_3O_4 nanoparticles via a fast and facile mechanochemical method: Modification of surface with porphyrin and photocatalytic study. *Mater. Lett.* **2016**, *166*, 247–250. [CrossRef]
31. Yu, J.; Zhu, S.; Pang, L.; Chen, P.; Zhu, G. Porphyrin-based magnetic nanocomposites for efficient extraction of polycyclic aromatic hydrocarbons from water samples. *J. Chromatogr. A* **2018**, *1540*, 1–10. [CrossRef] [PubMed]
32. Gross, Z.; Golubkov, G.; Simkhovich, L. Structural, electrochemical, and photophysical properties of gallium(III) 5,10,15-tris(pentafluorophenyl)corrole. *Angew. Chem.* **2000**, *39*, 4048–4051.
33. Girginova, P.I.; Daniel-da-Silva, A.L.; Lopes, C.B.; Figueira, P.; Otero, M.; Amaral, V.S.; Pereira, E.; Trindade, T. Silica coated magnetite particles for magnetic removal of Hg^{2+} from water. *J. Colloid Interface Sci.* **2010**, *345*, 234–240. [CrossRef] [PubMed]
34. Oliveira-Silva, R.; Pinto da Costa, J.; Vitorino, R.; Daniel-da-Silva, A.L. Magnetic chelating nanoprobes for enrichment and selective recovery of metalloproteases from human saliva. *J. Mater. Chem. B* **2015**, *3*, 238–249. [CrossRef]
35. Tavares, D.S.; Daniel-da-Silva, A.L.; Lopes, C.B.; Silva, N.J.O.; Amaral, V.S.; Rocha, J.; Pereira, E.; Trindade, T. Efficient sorbents based on magnetite coated with siliceous hybrid shells for removal of mercury ions. *J. Mater. Chem. A* **2013**, *1*, 8134–8143. [CrossRef]
36. Gryko, D.T.; Koszarna, B. Refined methods for the synthesis of meso-substituted A_3- and *trans*-A_2B-corroles. *Org. Biomol. Chem.* **2003**, *1*, 3–10. [CrossRef]